Investigations on the nature of observed ferromagnetism and possible spin polarization in Co-doped anatase TiO_2 thin films

D. H. Kim, J. S. Yang, K. W. Lee, S. D. Bu, D.-W. Kim,[a] and T. W. Noh[b]
ReCOE and School of Physics, Seoul National University, NS50, Seoul 151-747, Korea

S.-J. Oh
CSCMR and School of Physics, Seoul National University, NS50, Seoul 151-747, Korea

Y.-W. Kim
School of Materials Science and Engineering, Seoul National University, Seoul 151-744, Korea

J.-S. Chung
Department of Physics, Soongsil University, Seoul 156-743, Korea

H. Tanaka, H. Y. Lee, and T. Kawai
ISIR, Osaka University, Osaka 567-0047, Japan

J. Y. Won, S. H. Park, and J. C. Lee
Samsung Advanced Institute of Technology, Yongin-shi, Kyungki-do, Korea

(Received 2 December 2002; accepted 27 February 2003)

High-quality epitaxial thin films of Co-doped anatase TiO_2 (Co:TiO_2) were grown epitaxially on $SrTiO_3$ (001) substrates by using pulsed laser deposition with in-situ reflection high-energy electron diffraction. The oxygen partial pressure, P_{O2}, during the growth was systematically varied. As P_{O2} decreased, the growth behavior altered from a two-dimensional layer-by-layer-like growth to a three-dimensional island-like pattern. Electrical conductivity and saturation magnetization increased, seemingly consistent with the picture of carrier-induced ferromagnetism. However, we also found that the spatial distribution of Co ions became highly nonuniform and the chemical state of Co ions changed from ionic to metallic. All of these P_{O2} dependences, even including the transport and the magnetic properties, can be explained in terms of the formation of cobalt clusters, whose existence was clearly demonstrated by transmission–electron–microscope studies. Our work clearly indicates that the cobalt clustering will result in the room-temperature ferromagnetism observed in our Co:TiO_2 films. To check the possible spin polarization of carriers in Co:TiO_2 films, we also fabricated a heterojunction composed of a ferromagnetic Co:TiO_2, an insulating $SrTiO_3$, and a ferromagnetic half-metallic (La,Ba)MnO_3 layer. When the magnetic field was varied, we could not observe any changes in its I–V characteristic curves, which suggests that there might be little spin-polarization effect in the anatase Co:TiO_2 layer. © *2003 American Institute of Physics.* [DOI: 10.1063/1.1568524]

I. INTRODUCTION

The continuous attempts to develop next generation devices equipped with multifunctions are now being extended to the search for materials that can combine magnetic, electronic, and photonic responses.[1–9] One example of such efforts is to the quest for a ferromagnetic material system that can inject spin-polarized carriers into semiconductors. Ferromagnetic metals and alloys, such as Fe and FeNi, have been found to be inadequate, since spin-polarized carrier injection was found to be difficult due to resistance mismatch.[9] In attempts to overcome such problems, dilute magnetic semiconductors (DMS), such as (Ga,Mn)As, have emerged as good candidate materials.[1] Nowadays, numerous materials, including (Cd,Mn)GeP_2,[5] (Ga,Mn)N,[6] (Zn,Co)O,[7] and (Ga,Mn)P[8] are claimed to have room temperature ferromagnetism (FM). In spite of extensive efforts in this spintronics area, there has been a great deal of controversy, especially on fundamental issues such as the origins and characteristics of the observed FM.[3,4]

Recently, Matsumoto *et al.*[10,11] reported the occurrence of room temperature FM in Co-doped anatase TiO_2 (Co:TiO_2) films which were grown by combinatorial laser molecular beam epitaxy (MBE) techniques. This work generated great interest in the DMS community, since it could open up possibilities to create multifunctional oxides which utilize spin-polarized carriers.[11–20] Chambers *et al.*[12–14] reported magnetic and structural properties of the Co:TiO_2 films grown by the oxygen plasma-assisted MBE and claimed that the FM should be intrinsic. Park *et al.*[15] also reported that the polycrystalline Co:TiO_2 films grown by reactive co-sputtering of Co and Ti show ferromagnetic behavior at room temperature and claim that the Curie temperature should be higher than 400 K for samples with a Co content of 12%. On the other hand, Shinde *et al.*[17] measured the

[a]Present address: Samsung Advanced Institute of Technology, Yongin-shi, Kyungki-do, Korea.
[b]Electronic mail: twnoh@phya.snu.ac.kr

ion-channeling spectra and temperature-dependent magnetization of the Co:TiO_2 films grown by the pulsed laser deposition, and suggested that the FM arises from coexisting contributions of Co metal clusters and that of dispersed matrix-incorporated Co. More recently, we investigated the magnetic and microstructural properties of the anatase Co:TiO_2 films grown by laser MBE techniques. We found that Co nanoclusters could be formed at certain deposition conditions resulting in room temperature FM.[19]

In this article, we will provide more detailed physical properties and characterizations of Co:TiO_2 films grown under various oxygen partial pressures (P_{O2}. Namely, we will show that electrical resistivity, magnetic properties, chemical states, and compositional inhomogeneities can be systematically varied depending on P_{O2}. All of the observed P_{O2} dependences in our films can be explained by the formation of the Co nanoclusters in our epitaxial TiO_2 films. In addition, we will also present results on a multilayer junction composed of ferromagnetic $La_{0.9}Ba_{0.1}MnO_3$ (LBMO), insulating $SrTiO_3$ (STO), and ferromagnetic $Ti_{0.93}Co_{0.07}O_2$ layers. In some cases doping magnetic impurity atoms into the semiconductor matrix can result in the formation of ferromagnetic nanoclusters as well as the incorporation of a small fraction of these in the surrounding matrix to generate intrinsic DMS properties.[17,21] In this case, although the magnetic moment mostly comes from the ferromagnetic clusters, carriers in the matrix can be spin polarized.[21] However, our junction does not showed any magnetic field dependence, indicating that there should be little spin polarization of carriers in the anatase Co:TiO_2 layer of our multilayer junction.

II. EXPERIMENTS

Thin $Ti_{0.96}Co_{0.04}O_2$ (Co:TiO_2) films in the anatase phase were deposited on $SrTiO_3$ (001) substrates using the pulsed laser deposition method with *in situ* reflection high-energy electron diffraction (RHEED), which is known as the laser MBE.[22] A sintered polycrystalline $Ti_{0.96}Co_{0.04}O_2$ target was ablated by a KrF excimer laser (wavelength, 248 nm) with a fluence of 1.5 J/cm^2 at 2 Hz. The substrate temperature was maintained at 600 °C. P_{O2} was varied from 1.0×10^{-5} to 1.0×10^{-7} Torr. The growth rate was controlled to be extremely slow, less than 0.2 nm/min, which was reported to be necessary to reduce the Co inhomogeneity.[13] Thicknesses of the films used in this study were around 75 nm.

The Co:TiO_2/STO/LBMO multilayer junction was also prepared by the conventional pulsed laser deposition method to check the spin polarization of charge carriers of Co:TiO_2. All three layers were deposited *in situ* with the substrate temperature of 600 °C and at P_{O2} of 1.0×10^{-4} Torr. The relatively high P_{O2} was adapted to maintain proper oxygen stoichiometry of LBMO and STO during the *in situ* deposition. The growth rate was also controlled to be 1 nm/min, which is much higher than that of the laser MBE. (With the high deposition rate, we found that the ferromagnetic Co:TiO_2 films can be formed at higher P_{O2} than in the laser MBE case.)

Numerous characterization techniques were used to investigate the structural, electrical, magnetic, and chemical properties of the films. Structural properties were analyzed by high-resolution and conventional x-ray diffraction (XRD). For micro-structural analysis, cross-sectional transmission electron microscopy (XTEM) and energy-dispersive spectroscopy (EDS) were used. Electrical conductivities were measured with the conventional four-probe method. Magnetic properties were measured by a superconducting quantum interference device (SQUID) magnetometer. Co *K*-shell x-ray absorption near-edge fine structure (XANES) was used to measure chemical states of the dopant using the synchrotron source of the Pohang Accelerator Laboratory. Depth profiles of secondary ion mass spectrometry (SIMS) and Auger electron spectroscopy (AES) were also used to characterize the distribution of Co along the direction perpendicular to the film surface.

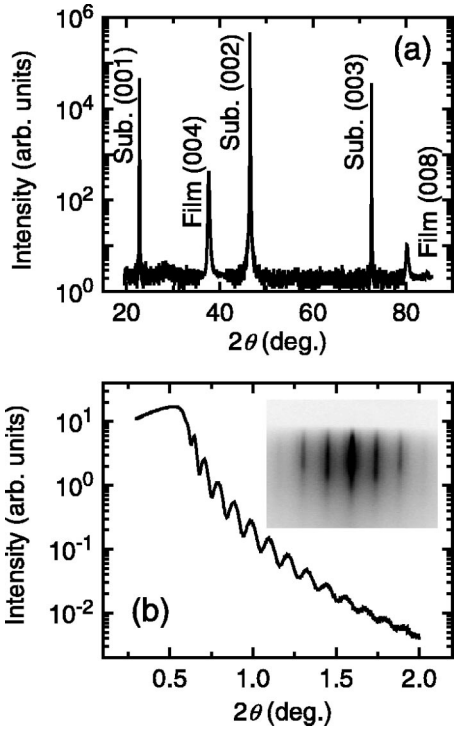

FIG. 1. (a) The XRD pattern and (b) the x-ray reflectivity curve of $Ti_{0.96}Co_{0.04}O_2$ film grown at $P_{O2}=1.0\times10^{-5}$ Torr at 600 °C on $SrTiO_3$ (001) substrate. The inset shows *in situ* RHEED patterns of the film.

III. RESULTS AND DISCUSSION

A. Ferromagnetism of Co:TiO_2 films

1. Growth of high-quality epitaxial anatase Co:TiO_2 film

The Co:TiO_2 films grown at an oxygen pressure of 1.0×10^{-5} Torr showed excellent structural properties. As shown in Fig. 1(a), the XRD pattern of the film shows only (00*l*) peaks of the anatase phase. A rocking curve of the (004) peak revealed a full width at half-maximum (FWHM) of 0.66°, which is similar to the value reported by Murakami *et al.*[23] X-ray reflectivity measurements were also performed with a high-resolution x-ray diffraction system. As shown in Fig. 1(b), its x-ray reflectivity curve showed oscillations coming from the parallelism of the film surface and the film/

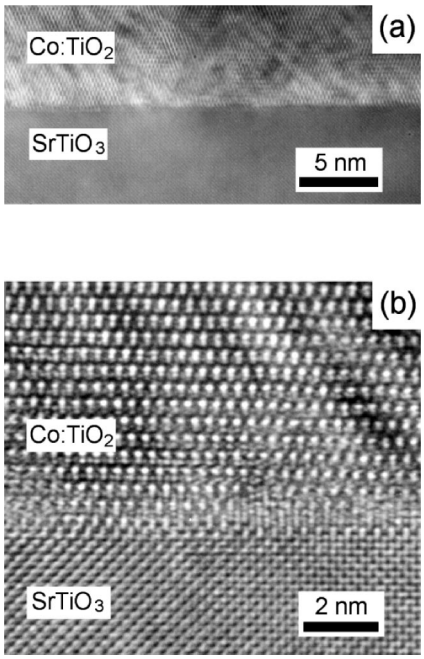

FIG. 2. (a) A high-resolution XTEM picture of the $Ti_{0.96}Co_{0.04}O_2$ film grown at a $P_{O2}=1.0\times10^{-5}$ Torr. (b) Magnified negative image of the same sample.

substrate interface. From the period of the oscillations, we could calculate the thickness of the film to be about 75 nm. The *in situ* RHEED pattern of the film, displayed in the inset of Fig. 1(b), shows a clear streaky pattern of the 1×4 reconstruction.[24]

The Co:TiO_2 thin films grown at P_{O2} of 1.0×10^{-5} Torr are of high quality and do not seem to contain observable segregation of impurity phases under XTEM. Figure 2(a) shows the TEM image of the Co:TiO_2 thin film grown at 1.0×10^{-5} Torr. It clearly shows corrugations from the atomic arrangements of the film and the substrate without any sign of segregation of impurity phases. Figure 2(b) shows a magnified negatively printed image, which displays a very sharp interface between the film and the substrate. There is no sign of segregation of impurity phases down to an atomic scale in this magnified image. These TEM images suggest that our films were epitaxially grown with high quality.

2. Effects of variation of oxygen partial pressure

Generally speaking, magnetic properties of DMS are known to be strongly dependent on carrier density. They are thought to have a close relationship with the origins of the magnetic exchange interaction that provides the observed ferromagnetic ordering in the DMS. Therefore, it has been considered important to systematically fabricate numerous DMS films, which have a large variation of carrier density (and/or electrical conductivity) without significantly altering other structural properties,[25] and to investigate their physical properties. For the anatase TiO_2 films, their electrical conductivities are known to come from oxygen vacancies.[26] Therefore, we tried to change their electrical conductivities by varying P_{O2} during growth.

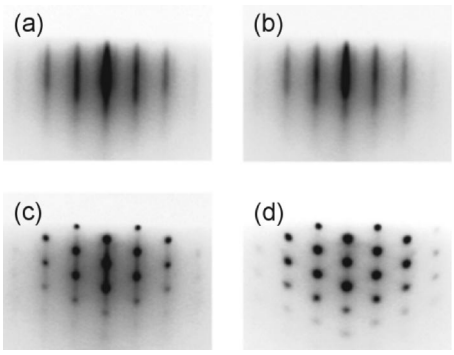

FIG. 3. The *in situ* RHEED patterns of the films which were grown under various oxygen partial pressures, $P_{O2}=1.0\times10^{-5}$ Torr, 3.3×10^{-6} Torr, 3.3×10^{-5} Torr, and 1.0×10^{-7} Torr for (a), (b), (c), and (d), respectively.

We found that the anatase TiO_2 films could be grown epitaxially under a wide range of oxygen partial pressure. Interestingly, we found an interesting growth mode change depending on P_{O2}: namely, the film growth mode will change from two-dimensional (2D) layer-by-layerlike growth to three-dimensional (3D) island growth. Figure 3 shows the final RHEED patterns of the anatase Co:TiO_2 films grown at four different values of P_{O2}. As P_{O2} decreases, the patterns change from two-dimensional streaky ones to three-dimensional spotty ones. As shown in Fig. 3(a), the film grown at 1.0×10^{-5} Torr shows a clear streaky RHEED pattern, suggesting a smooth surface. With decreasing P_{O2}, faint spots start to appear along the streaky pattern. For the film grown at 1.0×10^{-7} Torr, its RHEED pattern shows only spots, as in Fig. 3(d), which is known to represent a rough surface with three-dimensional (3D) island growth. The rough surfaces of the films with 3D-island growth were also confirmed by atomic force microscopy.

The variation in P_{O2} during growth seems to affect the lattice constants of the films along the *c*-axis, as shown in Fig. 4. The film with P_{O2} of 1.0×10^{-4} Torr has a *c*-axis lattice constant corresponding to the bulk value. As P_{O2} decreases to 1.0×10^{-5} Torr, the lattice constant starts to increase initially. This expansion can be explained by the introduction of oxygen vacancies that is known to expand the lattice constant. Further decrease of P_{O2} starts to cause the *c*-axis lattice constant to decrease. This behavior is rather difficult to understand precisely. However, it should be noted that the lattice constant could be relaxed due to the small-

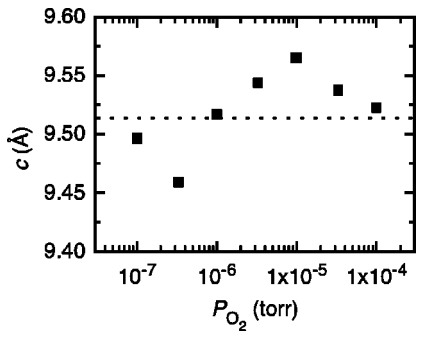

FIG. 4. The variation of lattice constants of the $Ti_{0.96}Co_{0.04}O_2$ films along their *c* axis vs P_{O2} at which they were grown.

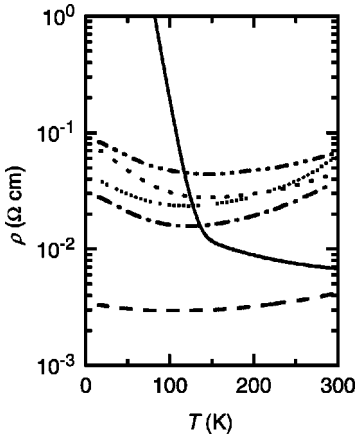

FIG. 5. Resistivity vs. temperature curves for the $Ti_{0.96}Co_{0.04}O_2$ films grown at various P_{O2}. The data for the films grown at 1.0×10^{-7}, 3.3×10^{-7}, 1.0×10^{-6}, 3.3×10^{-6}, 1.0×10^{-5}, and 1.0×10^{-4} Torr are shown as the solid, dashed, dashed–dotted, dotted, short dotted, and dashed–dotted–dotted curves, respectively.

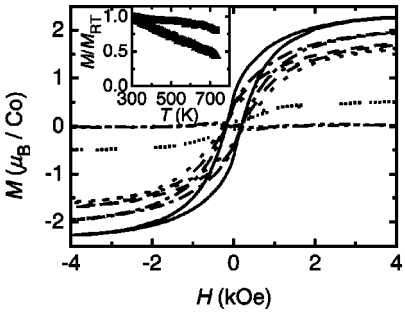

FIG. 6. Magnetization vs. magnetic field curves at 300 K for the $Ti_{0.96}Co_{0.04}O_2$ thin films under various P_{O2}. The data for the films grown at 1.0×10^{-7}, 3.3×10^{-7}, 1.0×10^{-6}, 3.3×10^{-6}, 1.0×10^{-5}, and 1.0×10^{-4} Torr are shown as the solid, dashed, dashed–dotted, dotted, short dotted, and dashed–dotted–dotted curves, respectively. The inset shows temperature dependence of the normalized magnetization for the films grown at P_{O2} of 1.0×10^{-7} Torr (the squares) and 1.0×10^{-5} Torr (the triangles).

angle grain boundary formation in the 3D-island growth regime. The FWHM of the anatase TiO_2 (004) peak in the rocking curve also increased to 0.86° at $P_{O2}=1.0\times10^{-7}$ Torr, compared to a value of 0.66° for the film grown at 1.0×10^{-5} Torr. This indicates that the film grown at lower P_{O2} has a wider mosaic spread, which is consistent with the change of the *c*-axis lattice constant.

Figure 5 shows that most films showed resistivity curves which have a metallic behavior near room temperature and an insulating response at low temperature. As P_{O2} is reduced, resistivity values are drastically lowered. The reduction in resistivity (or the increase in conductivity) might originate from the oxygen vacancies. With the cation in its 4+ state, TiO_2 is a well-known band insulator without electrons in the 3D band.[26] The oxygen vacancy could introduce two additional electrons in the Ti ion and they could move freely from one Ti ion to another, changing the band insulator into a metal. It is interesting to see that the resistance curve of the film grown at 1.0×10^{-7} Torr is quite different from those of other films, suggesting the possible formation of severe inhomogeneity in this sample.

Most of our films exhibit ferromagnetic properties at room temperature. Figure 6 shows magnetization vs magnetic field curves measured by SQUID at 300 K. Most films show clear ferromagnetic hysteresis loops at room temperature, except for the one that was grown at P_{O2} of 1.0×10^{-4} Torr. Magnetic properties of Co:TiO_2 films show a systematic change with P_{O2}. As P_{O2} decreases, the saturation magnetic moment increases.

B. Discussion on the origin of observed room temperature FM

1. Possibility of intrinsic effects

As we observed already, P_{O2} can result in systematic variation of the transport and magnetic properties. Figures 7(a) and 7(b) show the room temperature values of dc resistivity (ρ_{dc}) and saturation magnetization (M_S), respectively. As P_{O2} decreases, ρ_{dc} decreases and M_S increases. Assuming that more oxygen vacancies can be generated at lower P_{O2}, the systematic behavior of ρ_{dc} and M_S could be explained by the carrier-induced FM mechanism; namely, as more carriers are induced at lower P_{O2}, the magnetic interaction becomes stronger and results in FM. According to the Zener model,[27] which explains the exchange interaction between the magnetic impurity atoms in DMS as mediated by free charge carriers, the increase in charge carrier density can enhance the magnetic ordering.

However, there are some important behaviors which should be taken into consideration before drawing conclusions based on the carrier-induced FM mechanism. As shown in Fig. 7(b), with decreasing P_{O2}, M_S gradually increases but approaches the value of bulk cobalt ($1.7\mu_B$). Additionally, the magnetization versus temperature data, shown in the inset of Fig. 6, show that FM persists up to 750 K. In particular, for the film grown at $P_{O2}=1.0\times10^{-7}$ Torr, the magnetization does not decrease much with temperature. Note

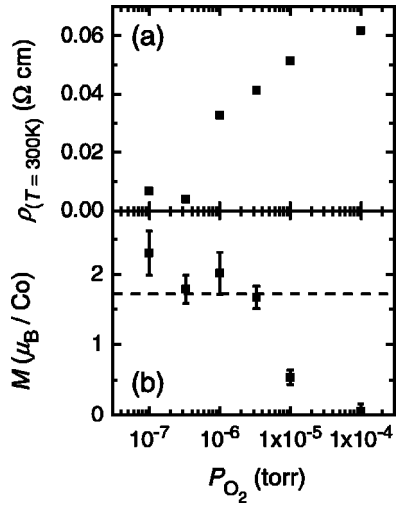

FIG. 7. (a) Dependence of the value of resistivity of the films at 300 K on P_{O2}. (b) Dependence of the saturation magnetization, M_S, of the $Ti_{0.96}Co_{0.04}O_2$ thin films on P_{O2}. The dotted line corresponds to the bulk value of cobalt metal.

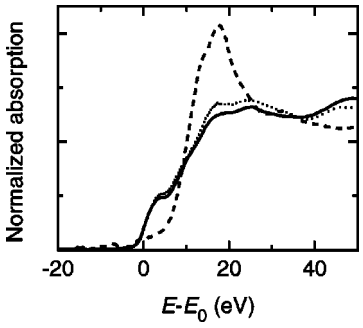

FIG. 8. Co *K*-edge XANES for the $Ti_{0.96}Co_{0.04}O_2$ thin films. Normalized Co *K*-edge absorption vs. effective photon energy (E-E_0) curves for the films grown at $P_{O2}=1.0\times10^{-7}$ Torr (the dotted line) and 1.0×10^{-5} Torr (the dashed line). The solid line is obtained from a reference of Co metal. E_0 corresponds to 7708.8 eV.

that the Curie temperature of metal Co is 1404 K. This high lower bound of the Curie temperature is rather difficult to explain in terms of the carrier-induced FM.

In the anatase TiO_2 films, which are in a metastable phase, the effects of inhomogeneous distribution of the Co atoms should be carefully considered. There are three different phases of TiO_2: rutile, anatase, and brookite. The most stable phase is rutile and they are used as optics and substrates in single crystalline form. Although the anatase phase is difficult to make in a bulk form, it is sufficiently metastable to be grown in thin film form on lattice matching substrates, such as $SrTiO_3$ and $LaAlO_3$.[23] Since the anatase phase is not thermodynamically stable, defects can be easily formed with a slight change in the film growth conditions. In addition, the Co ions are known to diffuse easily at a relatively low temperature, such as 400 °C.[20] Therefore, the possibility of formation of Co and/or Co-intermetallic clusters inside anatase TiO_2 film should be considered carefully in the case of oxide films grown at relatively high temperatures.

2. Evidence for cobalt nanoclustering

One of the critical issues pertaining to the Co-doped TiO_2 films is the chemical state of the Co ions. If the Co ions can exist as segregated metal clusters, we can explain the observed magnetism without recourse to the DMS descriptions. In Fig. 8, we show XANES spectra of the Co *K*-shell of films grown under P_{O2} of 1.0×10^{-5} and 1.0×10^{-7} Torr. In the spectrum of the film grown with P_{O2} of 1.0×10^{-5} Torr, there is a sharp peak at around 20 eV that indicates a $+2$ formal oxidation state for the Co ions.[14] However, for film grown under lower P_{O2}, its XANES spectrum is very similar to that of the Co metal. This indicates that, inside the film grown under the low P_{O2}, the Co ions do not exist in an oxidized state, but in the bulk metallic state.

It is also found that the distribution of the Co ions depends strongly on the growth condition. The depth profile of SIMS shows inhomogeneous distribution of Co, and changes with P_{O2}. As shown in Figs. 9(a) and 9(b), the distributions of Sr and Ti ions are almost the same regardless of the growth condition, respectively. However, Fig. 9(c) shows that in the films grown at low P_{O2}, the Co ions are located mostly at the interface between the film and the substrate.

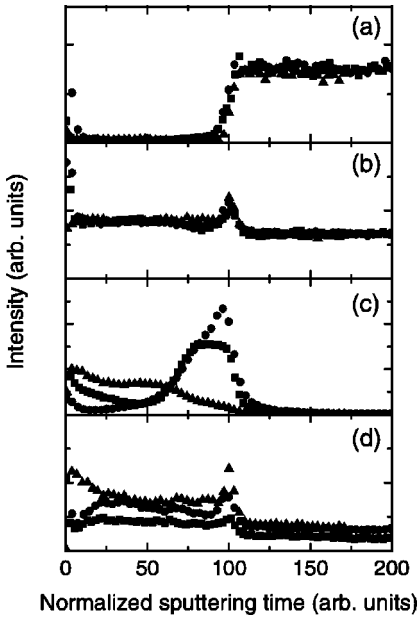

FIG. 9. (a) Depth profile of SIMS of the $Ti_{0.96}Co_{0.04}O_2$ thin films grown at $P_{O2}=1.0\times10^{-7}$ (squares), 3.3×10^{-7} (circles), and 1.0×10^{-5} Torr (triangles) for elemental Sr. Same data for elemental Ti, Co, and H are displayed in (b), (c), and (d), respectively.

The depth profiles of AES, which are not shown here, show similar results to those of SIMS. The high density of the Co ions near the interface suggests that they could be segregated to form clusters.

The XTEM image in Fig. 10 shows that the film grown under P_{O2} of 1.0×10^{-7} Torr has clusters of impurity phase. The clusters are distributed throughout the film but with a higher density at the interface. The observed distribution of clusters coincides with the SIMS result, shown in Fig. 9(c). The clusters located near or at the interface were larger in diameter than those in the middle of the film and the overall average diameter is 11.7 ± 6.0 nm. The density of the clusters is much higher at the interface, which can work as preferential nucleation sites due to its instability.

To identify the chemical composition of the observed clusters, we applied the EDS mapping technique. The TEM image in Fig. 11(a) shows clusters formed in the interface region. The apparent horizontal dark line, in the middle of

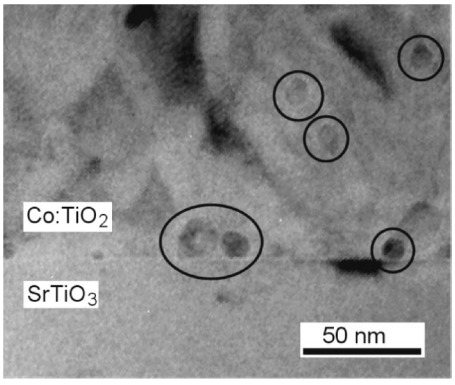

FIG. 10. An XTEM picture of the $Ti_{0.96}Co_{0.04}O_2$ film grown at $P_{O2}=1.0\times10^{-7}$ Torr.

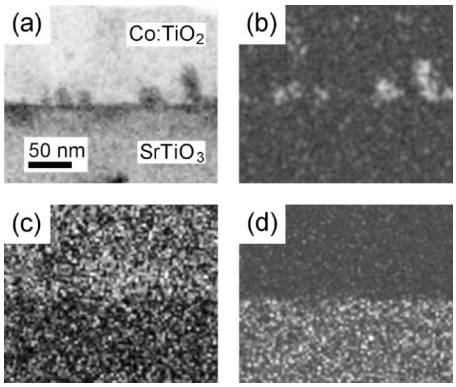

FIG. 11. (a) An XTEM picture and (b) the corresponding EDS mapping of elemental Co for the film grown at 1.0×10^{-7} Torr. Mapping of Ti and Sr are shown in (c) and (d), respectively. It can be easily seen that Co-rich nanoclusters were formed.

the Fig. 11(a), comes from the strain field induced by the lattice mismatch between the film and the substrate. With an EDS mapping, we can identify the distribution of a given element in Fig. 11(a). A mapping of elemental Ti, shown in Fig. 11(c), indicates that Ti is distributed throughout the image but with a higher density in the film than in the substrate. We can also see that the interface between high and low density of Ti coincides with that of the film and the substrate. In the case of the distribution of Sr, shown in Fig. 11(d), we can only see a dark area with some background noise in the film side and bright spots in the substrate side. This result is readily expected from the fact that Sr can be found only in the substrate. The Co mapping, in Fig. 11(b), shows that the positions of bright spots exactly coincide with those of the clusters, shown in Fig. 11(a). From this observation we can conclude that the nanoclusters are mainly composed of Co.

A high resolution XTEM image of a particle located at the interface region is shown in Fig. 12(a). On the left-hand side of the image, a circularly shaped particle or the segregation of impurity phase can be seen. Below the boundary that meets the bottom of the particle, STO substrate can be seen with its lattice fringes. Above the boundary, epitaxial TiO_2 (or Co:TiO_2) film surrounds the particle. At the top of the circular particle, Moiré fringes are clearly visible, suggesting that two crystals overlap. Moreover, the particle is found to be single crystalline. Under a higher magnification, the circular cluster is found to have lattice fringes with a spacing of 1.92 Å, which is equivalent to the spacing between the $(10\bar{1}1)$ planes of the bulk Co. Figure 12(b) shows mosaic spreads in the film with the nanoclusters. The spreads come from the lattice distortion by the clusters. This can explain the relaxation of the lattice constants along the *c* axis and the large FWHM value of the (004) peak for the anatase TiO_2 films grown under low P_{O2}. We can conclude that the observed inhomogeneities in the Co:TiO_2 films grown under P_{O2} of 1.0×10^{-7} Torr are mainly due to the formation of single-crystalline Co clusters.

The observed ferromagnetism of our Co:TiO_2 films and its dependence on the variation of P_{O2} during the growth, shown in Fig. 7(b), can be easily understood in terms of the formation of the Co nanoclusters. Under low P_{O2}, the cobalt

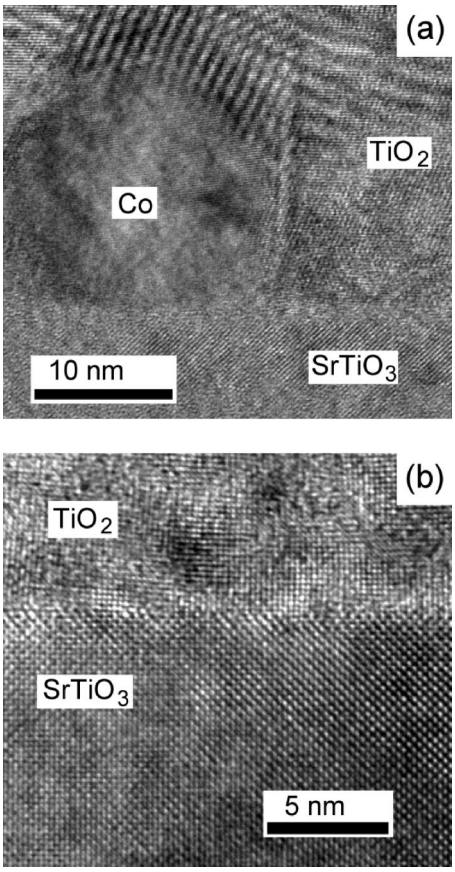

FIG. 12. (a) A high-resolution XTEM picture of the film with nanoclusters near the film/substrate interface. (b) Magnified picture at the film/substrate interface showing mosaic spread of the film due to formation of clusters.

oxide is less stable than TiO_2 from a thermodynamic point of view. The oxygen vacancies induced by low P_{O2} will help the diffusion of the Co atoms, resulting in the formation of the nanoclusters. As the number of Co clusters increases, the saturation magnetization will become larger. Although our TEM and XMCD work suggests that the nanoclusters should be mainly composed of Co, the cluster formation of other Co intermetallic compounds is not completely ruled out. As shown in Fig. 7(a), the value of saturation magnetization for the film grown at P_{O2} of 1.0×10^{-7} Torr is somewhat larger than that of bulk Co metal, which might be related to the formation of Co intermetallic compounds.

It should be noted that there still remains the possibility of ferromagnetism originated from intrinsic DMS effect in the Co-doped TiO_2 anatase films.[10–16] Our work just demonstrates that room-temperature ferromagnetism should be observed when Co nanoclusters are formed inside the TiO_2 films. In order to verify that the ferromagnetic properties observed in the Co-doped TiO_2 films are intrinsic, one should clearly demonstrate that the films have certain physical properties, such as anomalous Hall effects and/or x-ray magnetic circular dichroism, which cannot be explained simply by the Co clustering.[28] To the best of our knowledge, no such properties have been observed up to this point.

C. Properties of a Co:TiO_2 /insulator/FM-metal junction

To utilize DMS materials in practical spintronics applications, such as a spin injector, it is necessary for the carriers

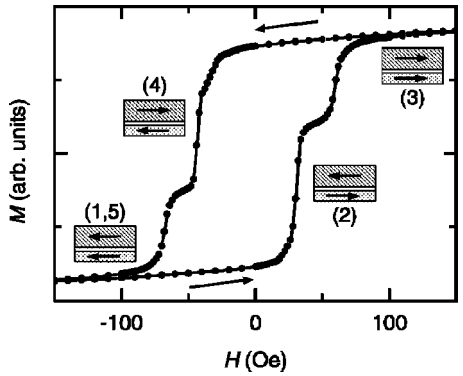

FIG. 13. Magnetic hysteresis curve of $Ti_{0.93}Co_{0.07}O_2/SrTiO_3/La_{0.9}Ba_{0.1}MnO_3$ multilayer measured at 10 K. Insets show the configuration of each layer's direction of magnetization under corresponding applied magnetic fields.

to have a spin polarization. Although the observed magnetic moments in the Co-doped TiO_2 films mainly originate from the Co nanoclusters, it might still be possible for the ferromagnetic particles to polarize the carriers inside the TiO_2 matrix. To investigate such a possibility, we constructed a multilayer junction composed of ferromagnetic $Ti_{0.93}Co_{0.07}O_2$, insulating $SrTiO_3$, and ferromagnetic $La_{0.9}Ba_{0.1}MnO_3$ (LBMO) metallic layers. LBMO is known to be a half-metal whose carriers are 100% polarized with a particular direction of spin.[29] At first, the LBMO film with a thickness of 15 nm was deposited on the STO substrate and the STO film with 30 nm thickness was deposited as an insulating barrier. Then, the Co:TiO_2 layer was deposited on top of them with a thickness of 500 nm.

Figure 13 shows the magnetic hysteresis curve of the multilayer junction measured at 10 K. This curve clearly shows that both top and bottom layers become ferromagnetic. With increasing magnetic field, there are rapid increases of magnetic moment around 30 and 60 Oe. Similar behavior can be observed in the field-decreasing run. This intriguing magnetic hysteresis curve can be explained by alignment of the ferromagnetic layers. Namely, 30 and 60 Oe correspond to values of the coercive fields of the LBMO and the Co:TiO_2 layers, respectively. As the magnetic field increases, the two ferromagnetic layers initially exhibit an antiparallel alignment, schematically drawn as the configuration (2) of Fig. 13. With a field larger than 60 Oe, they make a parallel alignment, shown as the configuration (3).

Figure 14(a) shows a schematic diagram to measure the magnetic-field-dependent I–V curves of the LBMO/STO/Co:TiO_2 multilayer junction, which can be interpreted as a p^+-i-n^+ diode. Note that the LBMO is well known to be a half-metal which has a 100% spin polarization. If there is a significant spin polarization in the ferromagnetic Co:TiO_2 layer, the tunneling currents between the layers should depend strongly on the directions of the magnetic moment. Figure 14(b) shows the I–V characteristics of the multilayer junction at 10 K at five different configurations, marked from (1) to (5) in Fig. 13. It is clear that there is little magnetic field dependence in the I–V curves. To see this more clearly, we plot the difference of the I–V characteristic curves for the configurations (4) and (5) in the inset

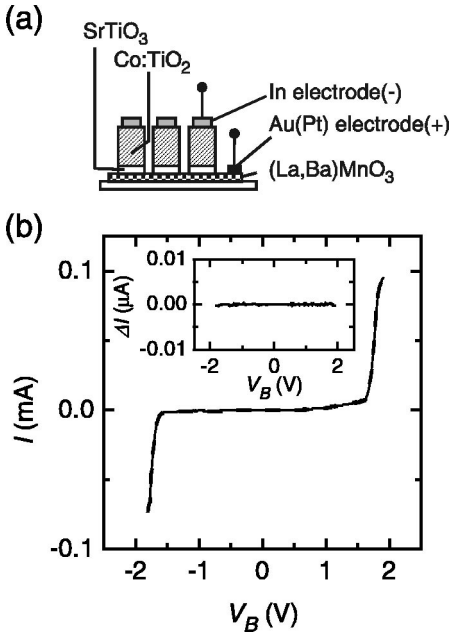

FIG. 14. Schematic diagram showing the configuration for measuring I–V curve of the multilayer junction. (b) I–V curves of the junction under the magnetic fields corresponding to four configurations shown in Fig. 13. All curves coincide and cannot be distinguished from others. The inset shows the difference between the curve under magnetic field at (1,5) and that at (4). This curve shows that there is no difference between the two curves except for a small amount of noise.

of Fig. 14(b). It shows that there is almost no difference except for a small amount of noise. In the negative bias region, the I–V curves show the Zener tunneling behavior. In the positive bias tunneling, the current seems to flow via a leakage current, showing a usual diffusion current behavior. If there is spin polarization in carriers in Co:TiO_2, TMR phenomena should be expected in this structure. We can expect that the current flows in the configurations (3) and (1,5) should have smaller resistance than those in the configurations (2) and (4). If the interfaces between the layers are clean, the observed weak magnetic field dependence of the I–V curves suggests that the carriers in the Co:TiO_2 layers should have no (or very little) spin polarization.

The magnetic properties of the thick Co:TiO_2 film in the multilayer junction seems to be quite different from those of the film at P_{O2} grown at the similar conditions by the laser MBE. Namely, the film grown at P_{O2} of 1.0×10^{-4} Torr by PLD has significant magnetization (i.e., about a half of the full magnetic moment of the metal Co), in contrast to the negligible magnetic moment of its counterpart, shown in Fig. 7(b). However, it should be noted that the deposition conditions of these two films were quite different. Chambers *et al.*[13] showed that the Co inhomogeneity could occur at a high deposition rate due to the high mobility of Co ions and claimed that a very slow deposition rate should be essential to grow homogeneous layer. Note that the deposition rate of our PLD growth is by a factor of 5 higher than that of the MBE grown samples. It is not clear at this moment whether the larger magnetic moment signal for the PLD grown sample come from clustering or other origins. It should be tested in a future. Even if the magnetic signal in the PLD

grown sample comes from some intriguing physical origin, the little magnetic field dependence of the *I–V* curves in our heterostructure seems to cast some doubts on usefulness of $Co:TiO_2$ film for applications of spin-polarized injection devices.

IV. SUMMARY

In summary, we grew high-quality anatase $Ti_{0.96}Co_{0.04}O_2$ films at various oxygen partial pressures. As the pressure was decreased, the growth behavior changed from a two-dimensional layer-by-layer-like growth to a three-dimensional island one, resulting in a rougher surface and a wider mosaic spread. The saturation magnetization also became increased. To identify the origin of such magnetization changes, we performed extensive investigations, including chemical status, special distribution, electrical distribution, and microstructural analysis. We found that the changes in the magnetic properties were closely related with the microstructural changes, which were due to the formation of cobalt nanoclusters. Although the possibility of other intrinsic origins cannot be completely ruled out, this work strongly suggests that the formation of Co clusters should comprise the main origin for the observed ferromagnetism, at least in our films. To check the possibility of spin polarization of carriers, we made a $La_{0.9}Ba_{0.1}MnO_3/SrTiO_3/Co:TiO_2$ multilayer junction. However, the *I–V* characteristics of this heterojunction do not show any dependence on magnetic field, indicating that the spin of carriers in our heterostructure could not be polarized.

ACKNOWLEDGMENTS

We wish to thank J. H. Park, Y. D. Park, and J.-G. Yoon for valuable discussions. We also thank H. C. Kim and H. C. Ri for the initial magnetization measurements at KBSI. This work was financially supported by KOSEF through CSCMR, and by the Ministry of Science and Technology through the Creative Research Initiative program. Experiments at Pohang Accelerator Laboratory were supported in part by MOST and POSCO.

[1] H. Ohno, Science **281**, 951 (1998).
[2] Y. D. Park, A. T. Hanbicki, S. C. Erwin, C. S. Hellberg, J. M. Sullivan, J. E. Mattson, T. F. Ambrose, A. Wilson, G. Spanos, and B. T. Jonker, Science **295**, 651 (2002).
[3] M. Berciu and R. N. Bhatt, Phys. Rev. Lett. **87**, 107203 (2001).
[4] A. Kaminski and S. Das Sarma, Phys. Rev. Lett. **88**, 247202 (2002).
[5] G. A. Medvedkin, T. Ishibashi, T. Nishi, and K. Hiyata, Jpn. J. Appl. Phys., Part 2 **39**, L949 (2000).
[6] M. L. Reed, N. A. El-Masry, H. H. Stadelmaier, M. K. Ritums, M. J. Reed, C. A. Parker, J. C. Roberts, and S. M. Bedair, Appl. Phys. Lett. **79**, 3473 (2001).
[7] K. Ueda, H. Tabata, and T. Kawai, Appl. Phys. Lett. **79**, 988 (2001).
[8] N. Theodoropoulou, A. F. Hebard, M. E. Overberg, C. R. Abernathy, S. J. Pearton, S. N. G. Chu, and R. G. Wilson, Phys. Rev. Lett. **89**, 107203 (2002).
[9] G. Schmidt, D. Ferrand, L. W. Molenkamp, A. T. Filip, and B. J. van Wees, Phys. Rev. B **62**, R4790 (2000).
[10] Y. Matsumoto, M. Murakami, T. Shono, T. Hasagawa, T. Fukumura, M. Kawasaki, P. Ahmet, T. Chikyow, S. Kohsihara, and H. Koinuma, Science **291**, 854 (2001).
[11] Y. Matsumoto, R. Takahashi, M. Murakami, T. Koida, X.-J. Fan, T. Hasegawa, T. Fukumura, M. Kawasaki, S.-Y. Koshihara, and H. Koinuma, Jpn. J. Appl. Phys., Part 2 **40**, L1204 (2001).
[12] S. A. Chambers, S. Thevuthasan, R. F. C. Farrow, R. F. Marks, J. U. Thiele, L. Folks, M. G. Samant, A. J. Kellock, N. Ruzycki, D. L. Ederer, and U. Diebold, Appl. Phys. Lett. **79**, 3467 (2001).
[13] S. A. Cahmbers, Materials Today **2002**(4), 34 (2002).
[14] S. A. Chambers, S. M. Heald, R. F. C. Farrow, J.-U. Thiele, R. F. Marks, M. F. Toney, and A. Chattopadhyay, cond-mat/0208315.
[15] W. K. Park, R. J. Ortega-Hertogs, J. S. Moodera, A. Punnoose, and M. S. Seehra, J. Appl. Phys. **91**, 8093 (2002).
[16] I.-B. Shim, S.-Y. An, C. S. Kim, S.-Y. Choi, and Y. W. Park, J. Appl. Phys. **91**, 7914 (2002).
[17] S. R. Shinde, S. B. Ogale, S. Das Sarma, S. E. Lofland, V. N. Kulkarni, J. Higgins, R. P. Sharma, R. L. Greene, and T. Venkatesan, cond-mat/0203576.
[18] J. R. Simpson, H. D. Drew, S. R. Shinde, Y. Zhao, S. B. Ogale, and T. Venkatesan, cond-mat/0205626.
[19] D. H. Kim, J. S. Yang, K. W. Lee, S. D. Bu, T. W. Noh, S.-J. Oh, Y.-W. Kim, J.-S. Chung, H. Tanaka, H. Y. Lee, and T. Kawai, Appl. Phys. Lett. **81**, 2421 (2002).
[20] J.-Y. Kim, J.-H. Park, B.-G. Park, H.-J. Noh, S.-J. Oh, J. S. Yang, D. H. Kim, S. D. Bu, T. W. Noh, H.-J. Lin, H.-H. Hsieh, and C. T. Chen, Phys. Rev. Lett. **90**, 017401 (2003).
[21] Y. D. Park, A. Wilson, A. T. Hanbicki, J. E. Mattson, T. Ambrose, G. Spanos, and B. T. Jonker, Appl. Phys. Lett. **78**, 2739 (2001).
[22] D.-W. Kim, D. H. Kim, B. S. Kang, T. W. Noh, D. R. Lee, and K.-B. Lee, Appl. Phys. Lett. **74**, 2176 (1999).
[23] M. Murakami, Y. Matsumoto, K. Nakajima, T. Makino, Y. Segawa, T. Chikyow, P. Ahmet, M. Kawasaki, and H. Koinuma, Appl. Phys. Lett. **78**, 2664 (2001).
[24] Y. Liang, S. Gan, S. A. Chambers, and E. I. Altman, Phys. Rev. B **63**, 235402 (2001).
[25] Y. Fukuma, H. Asada, M. Arifuku, and T. Koyanagi, Appl. Phys. Lett. **80**, 1013 (2002).
[26] H. Tang, K. Prasad, R. Sanjinès, P. E. Schmid, and F. Lévy, J. Appl. Phys. **75**, 2042 (1994).
[27] T. Dietl, H. Ohno, F. Matsukura, J. Cibert, and D. Ferrand, Science **287**, 1019 (2000).
[28] K. Ando cond-mat/0208010.
[29] T. Kanki, H. Tanaka, and T. Kawai, Phys. Rev. B **64**, 224418 (2001).